Towards Centimetre Accurate and Low-Power, Hybrid Radio-Acoustic 3D Indoor Positioning: an Experimental Journey.

1st Bert Cox
WaveCore, Department of Electrical Engineering (ESAT)
KU Leuven, Ghent Technology Campus
Ghent, Belgium
name.surname@kuleuven.be

2nd Chesney Buyle
WaveCore, Department of Electrical Engineering (ESAT)
KU Leuven, Ghent Technology Campus
Ghent, Belgium
name.surname@kuleuven.be

3rd Liesbet Van der Perre
WaveCore, Department of Electrical Engineering (ESAT)
KU Leuven, Ghent Technology Campus
Ghent, Belgium
name.surname@kuleuven.be

4th Lieven De Strycker
WaveCore, Department of Electrical Engineering (ESAT)
KU Leuven, Ghent Technology Campus
Ghent, Belgium
name.surname@kuleuven.be

***Abstract*—Battery powered asset trackers with a long device autonomy are a deep-rooted ambition for localisation solutions in retail, logistics and healthcare. This leaves a limited energy budget available for sensing, computing and communicating on the mobile sensor node. In this paper, we explore the attainable precision and accuracy in hybrid radio-acoustic, indoor 3D positioning for such energy-constrained devices. A state-of-the-art low-power ultrasonic-RF ranging technique is extended into a 3D indoor positioning system. The system is evaluated in a real-life measurement setup and over 30 000 measurements are captured. 2D advanced positioning estimation algorithms are adapted for the 3D application, and an in-depth comparison is performed. Positioning in favourable conditions shows that the Euclidean distance can be narrowed down to 0.0102 m. A road map with improvements on the hardware, algorithms and energy consumption is proposed to obtain this centimetre accuracy in the non-ideal situations. All data and algorithms are shared openly, encouraging ongoing research to test and improve their innovative positioning methods.**

***Index Terms*—Acoustic Sensors, Indoor Positioning, Low-Power Electronics, Ultrasonic Localisation**

I. Introduction

Positioning solutions in retail, logistics and healthcare aim for low-power asset tracking, as neglecting the power consumption results in a limited battery lifetime as well as higher maintenance and hardware costs. However, in the context of these emerging applications, the constrained energy budget should not counter the need for precise and accurate positioning. The approach for 3D positioning in this paper comes from this application-driven angle and tries to answer the following question: what accuracy can be obtained with energy-constrained sensor nodes?

Active ultrasonics is considered an attractive solution. Thanks to the relatively low propagation speed of sound, centimetre accurate positioning can be achieved without high-speed processing. The low system complexity and emerging MEMS microphone technology enable to create dedicated low-power and low-cost acoustic sensor nodes. The first series of mature, ultrasound positioning systems were presented around the year 2000. The leading-edge systems were the Active Bat system [1], [2], measuring the Time of Flight (ToF) of narrowband ultrasonic pulses and radio signals, and the Cricket system, [3], [4], using the Time Difference of Arrival between a simultaneous transmitted ultrasonic and RF signals. Although the narrowband ultrasonic pulses allow for simple architectures, they make the system highly receptive to in-band noise. Consequently, broadband signals were introduced shortly after [5], [6]. Through pulse compression, the effective bandwidth of the ultrasonic signals is increased, allowing the precision of the ranging measurement to be improved [7]. Pulse compression based on the cross-correlation of linear chirps has been widely adopted in the domain of ultrasound indoor positioning [8]–[11].

In more recent work, dedicated hardware to perform the positioning is eliminated by using smartphones [12], [13], as they are equipped with both a microphone and a speaker capable of receiving and producing acoustic signals that even go above the auditory range. Other sensors can be used on these devices, i.e. gyroscopes and accelerometers, enabling sensor fusion [14], [15], countering the high susceptibility of pure, acoustic ranging systems to room and environmental characteristics such as reverberation, Doppler shift and temperature.

In this work, we progress the state-of-the-art of 3D hybrid RF-acoustic positioning through three main contributions:

1) We extend the ultra-low hybrid RF-acoustic ranging strategy previously proposed in [11] and [16] into a 3D positioning system, targeting high precision and

reliable localisation of energy-constrained devices. The accuracy and precision are experimentally validated in an acoustically challenging environment. An extensive data set with over 30 000 measurements is made publicly available.
2) 2D advanced position estimation algorithms are adapted for 3D scenarios and compared based on the obtained real-life measurement data.
3) We provide a road map with technical advancements to further improve accuracy and reliability of energy-constrained indoor positioning systems.

A short introduction to the system architecture, ranging method and measurement setup is presented in the next section. Section III explores the measurement results and describes the used positioning methods. Next, a comparison between these algorithms is performed, to be finalised with a road map towards centimetre accuracy and a conclusion.

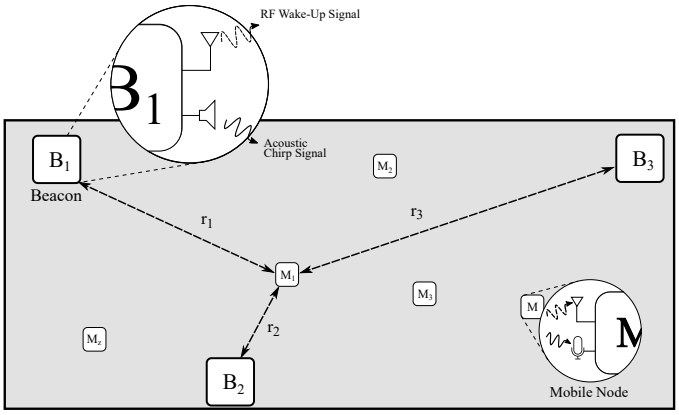

Fig. 1: 2D representation of indoor positioning system setup. Beacons periodically transmit ultrasonic chirps. All ultra low-power nodes are woken up and synchronised on basis of the RF signal.

II. Set-up

A. From Indoor Ranging to 3D Indoor Positioning

This study adopts the hybrid ranging system that is described in [11], [16] and depicted in Fig. 1. Distances between the two entity types, a fixed beacon and a mobile, sensor node, are calculated as follows:

1) A beacon sends out an ultrasonic audio chirp and RF wake-up signal.
2) Triggered by the RF signal, all mobile sensor nodes wake up simultaneous and sample audio for a limited amount of time (τ_{rx}).
3) The collected audio data are transmitted back to the beacon for further processing.

The ranging information is thus comprised in the received audio signal and depends on the distance to the beacon. At the sensor node, high frequency, bit based sampling eliminates the usage of a power hungry ADC and limits the amount of data that needs to be transmitted over the energy consuming RF connection. Distances are calculated by using binary template cross correlation, based on the matching procedure of Sokal [17] and by performing a peak-seeking procedure on the correlated data. The accuracy of this ranging method depends on the used chirp frequency bandwidth (Δf), the mobile sensor node wake-up time (τ_{rx}) and the binary sampling frequency ($f_{s,b}$). At the mobile sensor nodes, acoustic acquisition, amplification, binary sampling, packet handling and RF-communication are all done with 90.62 µJ. In this paper, we extend the aforementioned raging method into a 3D positioning system and evaluate the performance in a challenging real-life environment. Note that this method differs from typical propagation delay or round-trip time measurements in respectively synchronised and unsynchronised systems. It calculates the distance out of the pulse compression data instead of using an internal timer. Nevertheless, it provides the necessary ranges to perform true-range multilateration algorithms. It is generally known that at least four ranges are necessary for 3D-indoor positioning [18], leading to a setup expansion with a minimum of four beacons. A Time Division Multiple Access (TDMA) scheme is chosen to obtain the corresponding distances, as this prevents acoustic signal collision efficiently at the cost of a lower positioning update rate. With this, the main objective of this paper is to find a positioning method with the smallest mean 3D Euclidean distance at all test positions in the acoustically harsh set-up.

TABLE I: Average RT60 values of the Techtile room.

Frequency (Hz)	**125**	**250**	**500**	**1000**	**2000**	**4000**	**8000**
RT60 (s)	0.76	0.91	0.93	0.93	0.82	0.66	0.51
Uncertainty (%)	12.5	8.1	5.7	4.0	3.0	2.4	1.9

Fig. 2: Techtile test environment, a 8 x 6 x 2.4 m room consisting of 140 wooden tiles.

B. 3D Measurement Set-Up

All experiments are performed in the Techtile test environment [19] depicted in Fig. 2. This 8 x 6 x 2.4 m room, comprising 140 modular wooden tiles, represents a real-life, acoustically harsh environment, with high reverberation time (Table I). Four acoustic beacons are spread across the test bed, with three of them close to the outer edges of the room, maximising the spatial resolution on all three axes.

Each beacon consists of an ultrasonic speaker (Kemo L010) directed to the centre of the room and an off-the-shelf amplifier with a frequency range over 45 kHz. These four beacons are connected to a multi-channel DAC [20], where the chirp signals are generated and TDMA beacon selection is performed. The sensor node consists of a single MEMS microphone with distinctive amplifier and band filter combined with a sub-GHz wireless MCU launchpad [21]. A central computer connected to another launchpad handles the received binary sampled audio chirps and calculates the measured distances.
Measurements are performed on 150 fixed positions: each of the three layers consists of a uniform planar array of 50 points. On each position at least 50 distances are measured to each of the four beacons, resulting in a total of over 30 000 ranging measurements. These time expanded ranging measurement are necessary to average out errors introduced by the dynamic Techtile environment.

III. Measurements, Processing, and Interpretation

A. Ranging in a challenging environment

To understand the potential positioning inaccuracies and single out advanced positioning algorithms, we first explore the ranging measurements. A helpful data visualisation technique for errors between the actual and measured distance is a heat map, displaying the error range's magnitude in a 2D projection of the room. Fig. 3 displays four such heat maps, one for each beacon, showing the Mean Absolute Error (MAE) of 50 positions on a fixed height (Z = 1.406 m). The speaker position and orientation are illustrated by a symbol. A couple of observations can be made. Firstly, the error increases with the distance. This can be attributed to signal attenuation and can be easily described with the inverse square law. In this system lower signal-to-noise ratio's are detrimental for the zero-crossing based, binary template cross correlation. Secondly, larger errors can be found closer to the edge of the room. A potential hypothesis can be found in the high reverberation time of the room. And thirdly, in all four heat maps, a directional speaker pattern can be noticed. To clarify the latter two, a more elaborate statistical analysis and extra measurements are performed.
Table II gives more insight in the accuracy and precision of the distance measurements between a single beacon and a sensor node close to a wall. To measure the influence of reverberation, two sets of 140 ranging measurements were conducted on the same position, one with and another without acoustic absorbers added on the nearest wall. The median (μ), difference between mininmum and maximum value (range), mean (P50), P95 and standard deviation (σ) values of 140 measurements on the same location are all spectacularly improved when absorbers are added, cancelling out reflections and decreasing the reverberation locally. In this case, the low median and mean distance error values result in a high accuracy whilst the standard deviation of only 5.2 cm and range of 22.8 cm reveal a small error variation with low outliers and thus a high precision. To evaluate the influence of the speaker, a far-field, 2D speaker directivity measurement was performed. The normalised polar plot with an angular resolution of 1° for a sine wave of 25 kHz can be found in Fig. 4. A half power beam width of 40° confirms the directionality hypothesis.
These ranging results are promising, with centimetre-accuracy given favourable circumstances. Yet it will be interesting how well the 3D positioning algorithms perform for mobile sensor nodes close to walls or out of the main acoustic lobes.

TABLE II: Influence of acoustic absorbers on the absolute distance error for a sensor node close to a wall.

	μ (m)	Range (m)	P50 (m)	P95 (m)	σ (m)
Absorber	0.083	0.228	0.087	0.179	0.052
No absorber	0.958	1.965	0.971	1.938	0.894

B. Indoor Positioning and estimate optimisation algorithms

Range-based positioning optimisation is intrinsically finding a position estimate with the smallest error term explaining all the distance measurements. This is often achieved by solving a set of nonlinear equations in a least square sense. A fair simulation-based comparison of different iterative and closed-form nonlinear algorithms for 2D positioning can be found in [22]. We have adapted these algorithms for a 3D environment and extended the simulations with experimental data from ranging measurements. This section gives an overview of the implemented algorithms accompanied with a short explanation. For a full derivation and description we refer to the original papers. Notations are the same in all algorithms with:

- s_i is the position vector of beacon i containing its x, y and z coordinates
- N is the number of beacons (4)
- r_i is the ranging measurement to beacon i
- $\hat{p}$ is the position estimate

The pseudocode of the algorithms can be found in Appendix A. The Python implementation of the distance measurement, positioning algorithms and the data sets can be found in [23].

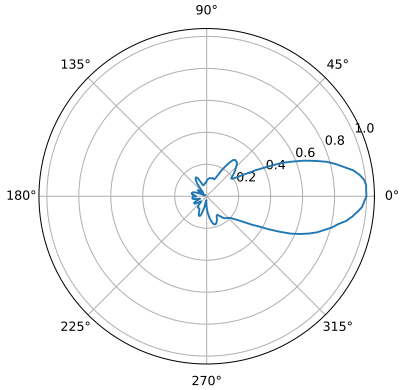

Fig. 4: Polar plot of the normalised XY directionality of the Kemo L010 @25 kHz in non-anechoic chamber.

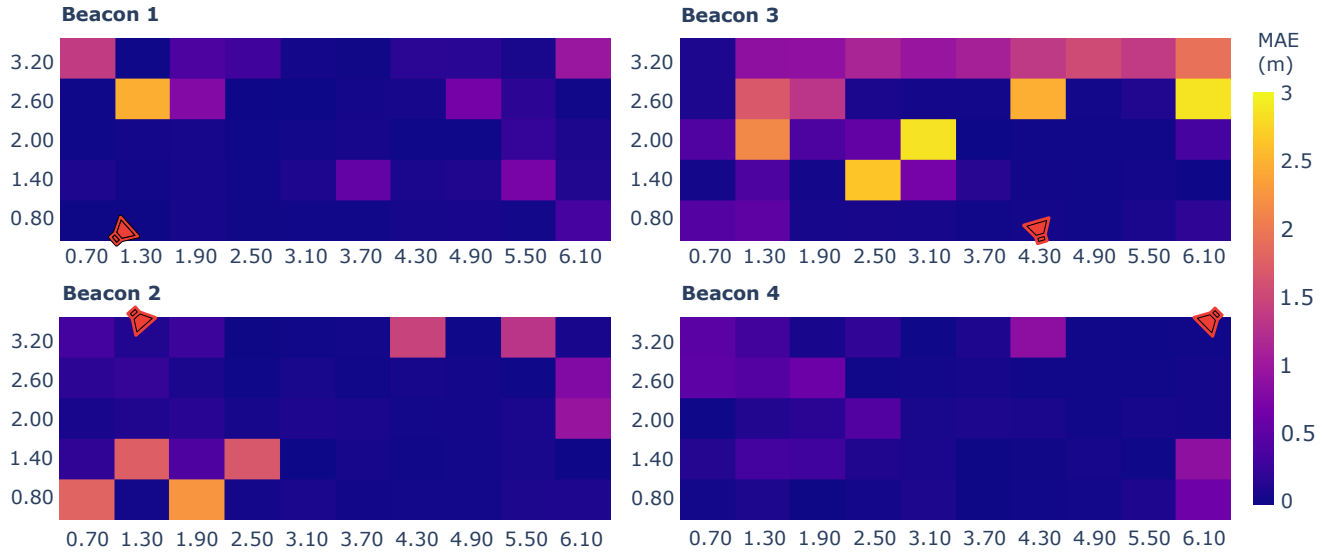

Fig. 3: Mean absolute distance error heat maps for ranging to different beacons at a height of 1.407 m.

1) Simple Intersection: Classical multilateration interpret the measured ranges as circles centred around the beacon. The combination of several of these circular 'lines of positions' (LOPs), generate an intersection. The latter is than considered to represent the best estimate for the position of the mobile sensor node. This geometrical approach is susceptible to noise. As errors are introduced, the circular LOPs do not intersect in a specific point, but create an area with potential estimates. In [24], linear LOPs are created by drawing a straight line through the intersecting points of two ranging circles. The intersection of these newly generated lines indicates the position estimation. The advantage of this method is that it is still possible to generate linear LOPs when, due to errors, two or more circles do not intersect. The Moore-Penrose inverse, least squares estimate can be used to find an algorithmic rather than a geometric solution with a minimum number of linear LOPs of $N-1$.

2) Bancroft: [25] uses an algebraic, non-iterative technique to solve the GPS equations that is computationally efficient and numerically stable. In contrast to iterative techniques, higher order terms of the Taylor series expansions are not discarded, resulting in a better performance when beacons are poorly arranged. Although there is a lot of similarity with the Simple Intersection method, the Moore-Penrose inverse is not used for minimising the difference between the exact position and measurement residual, but as a projection operator in the n-dimensional space of these residuals.

3) Beck: Instead of a range-based least squares (R-LS) minimisation, a squared-range-based least squares method (SR-LS or least quartic) can be used to find a position estimate [26]. An exact, optimal solution can be found by using a bisection algorithm to find a single root of a univariate strictly monotonous function. This method shows a better mean squared position error in comparison with the R-LS method.

4) Chueng: An alternative way to compute the SR-LS estimate is presented in [27]. For a 3-dimensional space, all roots of a seven root equation are calculated by rewriting it in a seventh degree polynomial. In contrast with the original paper, the absolute of the roots are taken instead of eliminating complex roots. The root closest to zero is used to compute the estimate of the globally optimal constrained weighted least squares.

5) Gauss-Newton: also known as Weighted Iterative Least Squares (WILS) is a straightforward method using only algebraic operations, in the form of a Jacobian matrix or the derivative of the measurement equation, to find an estimation. The disadvantages of this method are the need for prior information in the form of a initial positioning guess and the fact that it is computationally harder. [22] suggests the simple intersection method as a starting point for the position estimation. When used in time series, the algorithm extends naturally to a Kalman filter.

C. Empirical Comparison

To compare the different 3D position estimation algorithms, we have generated the Cumulative Density Function (CDF) of the mean Euclidean distance of 50 measurement in each of the 150 positions for the different methods, as plotted in Fig. 5. At first glance, it is clear that implementing more advanced estimation algorithms greatly improves the position estimation. When taking a closer look, we can divide the plots into three groups. The first one is the Chueng method, showing the steepest incline and outperforming all the other algorithms. With half the measurements below a distance of 0.73 m and 95% just above the 1.54 m, it demonstrates to be accurate even with erroneous ranging measurements. The three methods belonging to the second group are Bancroft, Beck and Gauss-Newton. They have a similar curvature and a P90 value below 3.5 m, with the Gauss Newton method having a single outlier at 69.8 m. The last curve consists of the basic intersection

method, with a low accuracy and high susceptibility to noise (P90 of 10.34 m).

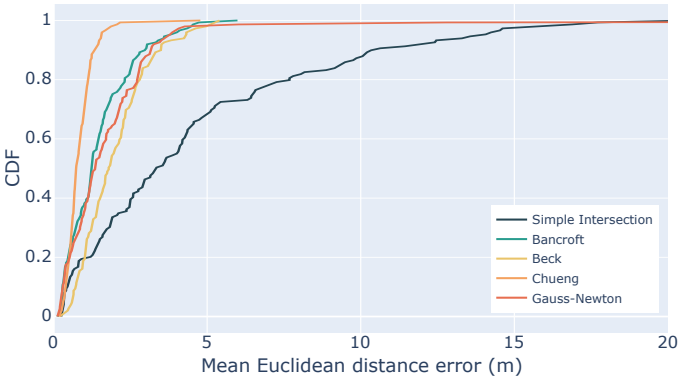

Fig. 5: Cumulative density functions of the mean Euclidean distance error over 50 measurements at the 150 different positions.

To investigate the influence of the ranging error on the precision, the position estimates of the two best performing position estimation techniques are plotted in Fig. 6. Two scenario's are depicted, with the yellow dot representing the actual position. The sensor node position in the first scenario is closer to the wall, with larger average distance measurement errors to two beacons: 0.923 m and 0.626 m to respectively beacon 1 in the upper left corner, and beacon 4, at the far right. The second sensor node position is more centred, and has a maximum mean ranging error below 5 cm. The Chueng algorithm behaves similarly in both scenarios: forming a dense cloud in the neighbourhood of the actual position. The mean Euclidean distance is 0.490 m for the first scenario and 0.554 m for the second. This indicates a lower accuracy, while at the same time having a high precision for both scenarios, hence the dense cloud. The Bancroft forms a more scattered arrangement, performing worse on both accuracy and precision. Even with precise distance measurements, the estimates spread out in the z-direction, where the beacon range resolution is lowest.

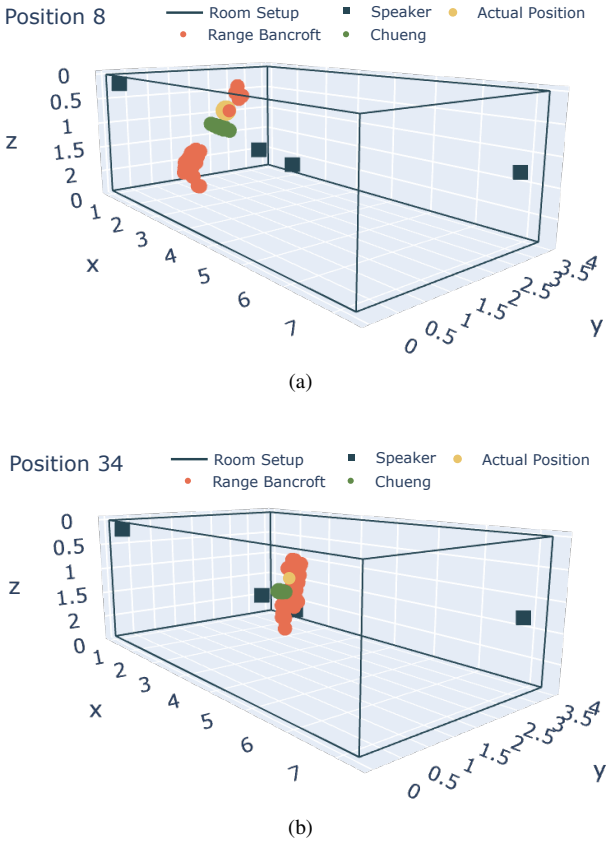

(a)

(b)

Fig. 6: Position estimations of the Chueng and Bancroft method on two positions.

IV. The road towards centimetre accuracy

In the most favourable conditions, the Euclidean distance is 0.0102 m, indicating that the intended accuracy *can* be achieved. Undeniable, the system still needs further improvement to reach this centimetre accuracy in non-ideal conditions, and the error to be bridged is at least an error of magnitude? Undeniable, there is still a road to go to reach this centimetre accuracy in non-ideal conditions, and the error to be bridged is at least an order of magnitude. For more consistent exact location estimates of energy-constraint nodes, we propose the following promising upgrades:

- **Hardware and system based improvements.** To prevent signal attenuation due to speaker directivity, the system could be extended on a hardware level by adding extra speakers to the beacons. Care should be taken in the design, as constructive interference and spatial aliasing occur at higher frequencies when multiple speakers are used, resulting in non-uniform and, again, directional sound pressure fields [28]. Beacon placement should be optimised as well, potentially increasing the number of beacons. Even with precise ranging measurements, positioning errors are largest in the z-dimension of the room. The resolution on this axis can be increased by placing a beacon in the ceiling or embed it in the floor. When such beacons are added to the system, adaptive beacon selection algorithms could be implemented to minimise the amount of active anchors and increase the position reliability.
- **Improve, combine or implement new positioning algorithms.** The chosen optimisation algorithms can be considered as safe and credible. They are an excellent way to test the feasibility of the system at the cost of accuracy and precision. We strongly believe that progress can be made if this research is extended with more recent positioning methods. Advanced position estimation techniques could be combined. Algorithms like non-linear least square estimation and Gauss-Newton require an initial positioning guess. In this paper, the poorly performing simple intersection method is used as a starting point as suggested by [22]. Future research could explore the

Chueng algorithm as a starting point or investigate the potential accuracy gain of time-series Kalman filters.

- **Reduce the distance measurement error.** Current processing uses the index of maximum correlation peak for the distance calculations. [11] shows that interference of higher frequencies can cause correlation peaks larger than the actual distance correlation maximum. Peak prominence and window functions can help selecting the correct local maximum and reduce the ranging error drastically.
- **Tackle the position update rate and mobile node energy consumption.** Current TDMA implementation gives a positioning update every 4 seconds with an energy consumption of 362.45 µJ. Increasing the ranging frequency solves the positioning update rate as long as multi-user interference is prevented. To lower the energy consumption, a better solution would be to simultaneously transmit the acoustic signals. In [29], [30] a Chirp Spread Spectrum (CSS) transmission scheme is introduced, enabling multi-user communication. A more in-depth study should validate the bit based sampling for this latter method.

V. Conclusion

In the present study, we extended a state-of-the-art RF-acoustic ranging strategy into a low-power, 3D positioning system. Four existing advanced 2D position estimation algorithms have been adapted to operate in 3D. Their performance has been assessed and compared based on the actual distance measurement data in an acoustically challenging environment. With these constrains, a median Euclidean distance error below 0.75 m was obtained. Current TDMA implementation results in a sensor node consumption of only 362.45 µJ for a single position estimate. In further research we aim to improve the energy consumption and positioning accuracy by adapting the infrastructure, combining or implementing (new) optimisation algorithms and researching multiple access methods. The data of over 30 000 ranging measurements and applied position estimation algorithms are shared openly, encouraging ongoing research to test and improve their innovative positioning methods.

References

[1] A. Ward, A. Jones, and A. Hopper, "A new location technique for the active office," *IEEE Personal Communications*, vol. 4, no. 5, pp. 42–47, 1997.

[2] M. Addlesee, R. Curwen, S. Hodges, J. Newman, P. Steggles, A. Ward, and A. Hopper, "Implementing a sentient computing system," *Computer*, vol. 34, no. 8, pp. 50–56, 2001.

[3] N. B. Priyantha, A. Chakraborty, and H. Balakrishnan, "The cricket location-support system," in *Proceedings of the 6th Annual International Conference on Mobile Computing and Networking*, ser. MobiCom '00. New York, NY, USA: Association for Computing Machinery, 2000, p. 32–43. [Online]. Available: https://doi.org/10.1145/345910.345917

[4] N. B. Priyantha, "The cricket indoor location system," Ph.D. dissertation, USA, 2005.

[5] M. Hazas and A. Hopper, "Broadband ultrasonic location systems for improved indoor positioning," *IEEE Transactions on Mobile Computing*, vol. 5, no. 5, pp. 536–547, 2006.

[6] J. R. Gonzalez and C. J. Bleakley, "High-precision robust broadband ultrasonic location and orientation estimation," *IEEE Journal of Selected Topics in Signal Processing*, vol. 3, no. 5, pp. 832–844, 2009.

[7] J. A. Paredes, F. J. Álvarez, T. Aguilera, and J. M. Villadangos, "3d indoor positioning of uavs with spread spectrum ultrasound and time-of-flight cameras," *Sensors*, vol. 18, no. 1, 2018. [Online]. Available: https://www.mdpi.com/1424-8220/18/1/89

[8] S. I. Lopes, J. M. N. Vieira, and D. Albuquerque, "High accuracy 3d indoor positioning using broadband ultrasonic signals," in *2012 IEEE 11th International Conference on Trust, Security and Privacy in Computing and Communications*, 2012, pp. 2008–2014.

[9] C. Medina, J. C. Segura, and A. De la Torre, "Ultrasound indoor positioning system based on a low-power wireless sensor network providing sub-centimeter accuracy," *Sensors*, vol. 13, no. 3, pp. 3501–3526, 2013. [Online]. Available: https://www.mdpi.com/1424-8220/13/3/3501

[10] M. O. Khyam, M. J. Alam, A. J. Lambert, M. A. Garratt, and M. R. Pickering, "High-precision ofdm-based multiple ultrasonic transducer positioning using a robust optimization approach," *IEEE Sensors Journal*, vol. 16, no. 13, pp. 5325–5336, 2016.

[11] B. Cox, L. Van der Perre, S. Wielandt, G. Ottoy, and L. De Strycker, "High precision hybrid rf and ultrasonic chirp-based ranging for low-power iot nodes," *EURASIP Journal on Wireless Communications and Networking*, vol. 2020, no. 1, p. 187, Sep. 2020.

[12] F. Hoflinger, R. Zhang, J. Hoppe, A. Bannoura, L. M. Reindl, J. Wendeberg, M. Buhrer, and C. Schindelhauer, "Acoustic self-calibrating system for indoor smartphone tracking (assist)," in *2012 International Conference on Indoor Positioning and Indoor Navigation (IPIN)*, 2012, pp. 1–9.

[13] H. Murakami, M. Nakamura, H. Hashizume, and M. Sugimoto, "3-d localization for smartphones using a single speaker," in *2019 International Conference on Indoor Positioning and Indoor Navigation (IPIN)*, 2019, pp. 1–8.

[14] S. Perez-Bachiller, D. Gualda, M. C. Perez, J. M. Villadangos, J. Urena, and R. Cervigon, "Android application for indoor location using sensor fusion: Ultrasounds and inertial devices," in *2018 International Conference on Indoor Positioning and Indoor Navigation (IPIN)*, 2018, pp. 1–8.

[15] D. Gualda, M. C. Perez-Rubio, J. Urena, S. Perez-Bachiller, J. M. Villadangos, A. Hernendez, J. J. Garcia, and A. Jimenez, "Locate-us: Indoor positioning for mobile devices using encoded ultrasonic signals, inertial sensors and graph-matching," *Sensors*, vol. 21, no. 6, 2021.

[16] B. Cox, L. Van der Perre, and L. De Strycker, "Zero-crossing chirp frequency demodulation for ultra-low-energy precise hybrid rf-acoustic ranging of mobile nodes," *IEEE Sensors Letters*, vol. 4, no. 5, pp. 1–4, 2020.

[17] R. R. Sokal, "The principles and practice of numerical taxonomy," *Taxon*, vol. 12, no. 5, pp. 190 – 199, Jun. 1963.

[18] A. Kupper, *Location-based services : fundamentals and applications.* Chichester: Wiley, 2005.

[19] G. Callebaut, J. V. Mulders, G. Ottoy, and L. V. der Perre, "A primer on techtile: An r&d testbed for distributed communication, sensing and positioning," 2021.

[20] *USB-6212: 16 AI (16-Bit, 400 kS/s), 2 AO (250 kS/s), Up to 32 DIO USB Multifunction I/O Device*, National Instruments, 2017, rev.

[21] *SimpleLink Sub-1 GHz CC1310 wireless MCU LaunchPad development kit*, Texas Instruments, 2018, rev. A.

[22] N. Sirola, "Closed-form algorithms in mobile positioning: Myths and misconceptions," in *2010 7th Workshop on Positioning, Navigation and Communication*, 2010, pp. 38–44.

[23] B. Cox, "Hybrid 3d-positioning," May 2021. [Online]. Available: https://github.com/BertCox/Hybrid3DPositioning

[24] J. Caffery, "A new approach to the geometry of toa location," in *Vehicular Technology Conference Fall 2000. IEEE VTS Fall VTC2000. 52nd Vehicular Technology Conference (Cat. No.00CH37152)*, vol. 4, 2000, pp. 1943–1949 vol.4.

[25] S. Bancroft, "An algebraic solution of the gps equations," *IEEE Transactions on Aerospace and Electronic Systems*, vol. AES-21, no. 1, pp. 56–59, 1985.

[26] A. Beck, P. Stoica, and J. Li, "Exact and approximate solutions of source localization problems," *IEEE Transactions on Signal Processing*, vol. 56, no. 5, pp. 1770–1778, 2008.

[27] K. Cheung, H. So, W.-K. Ma, and Y. Chan, "Least squares algorithms for time-of-arrival-based mobile location," *IEEE Transactions on Signal Processing*, vol. 52, no. 4, pp. 1121–1130, 2004.
[28] C. Quested, A. Moorhouse, B. Piper, and B. Hu, "An analytical model for a dodecahedron loudspeaker applied to the design of omni-directional loudspeaker arrays," *Applied Acoustics*, vol. 85, pp. 161–171, 2014.
[29] F. Yuan, Q. Wei, and E. Cheng, "Multiuser chirp modulation for underwater acoustic channel based on vtrm," *International Journal of Naval Architecture and Ocean Engineering*, vol. 9, 10 2016.
[30] C. Bernard, P.-J. Bouvet, A. Pottier, and P. Forjonel, "Multiuser chirp spread spectrum transmission in an underwater acoustic channel applied to an auv fleet," *Sensors (Basel, Switzerland)*, vol. 20, no. 5, p. 1527, Mar 2020.

APPENDIX A
ALGORITHMS

[BERT: To do: algorithm spacing]

Algorithm 1 Simple Intersection

$$A = \begin{bmatrix} 2s_1^T \\ \vdots \\ 2s_4^T \end{bmatrix}, \quad b = \begin{bmatrix} \|s_1\|^2 - r_1^2 \\ \vdots \\ \|s_4\|^2 - r_4^2 \end{bmatrix}$$
$$D = \begin{bmatrix} -1 & I_{N-1} \end{bmatrix}$$

with I_{N-1} the identity matrix gives:

$$\hat{p} = \left(A^T D^T D A\right)^{-1} A^T D^T D b$$

Algorithm 2 Bancroft

$$A = \begin{bmatrix} 2s_1^T \\ \vdots \\ 2s_4^T \end{bmatrix}, \quad b = \begin{bmatrix} \|s_1\|^2 - r_1^2 \\ \vdots \\ \|s_4\|^2 - r_4^2 \end{bmatrix}$$
$$v = \left(A^T A\right)^{-1} A^T \mathbf{1}$$
$$w = \left(A^T A\right)^{-1} A^T b$$

find the roots of:

$$\|v\|^2 t^2 + \left(2v^T w - 1\right) t + \|w\|^2 = 0,$$

and from the two position candidates:

$$\hat{p}_i = v t_i + w, \quad i = 1, 2$$

pick the one with the smallest residual as the final estimate.

Algorithm 3 Beck

$$A = \begin{bmatrix} 2s_1^T & -1 \\ \vdots & \\ 2s_4^T & -1 \end{bmatrix}, \quad b = \begin{bmatrix} \|s_1\|^2 - r_1^2 \\ \vdots \\ \|s_4\|^2 - r_4^2 \end{bmatrix}$$
$$P = \begin{bmatrix} 1 & 0 & 0 & 0 \\ 0 & 1 & 0 & 0 \\ 0 & 0 & 1 & 0 \\ 0 & 0 & 0 & 0 \end{bmatrix}, \quad q = \begin{bmatrix} 0 \\ 0 \\ 0 \\ -\frac{1}{2} \end{bmatrix}$$

Use a bisection method to obtain a solution for

$$\phi(\lambda) = \hat{z}(\lambda)^T P \hat{z}(\lambda) + 2q^T \hat{z}(\lambda)$$

in the declining interval $[-1/\lambda_1, \infty]$, where

$$\lambda_1 = \max\left(\text{eig}\left(A^T A\right)^{-\frac{1}{2}} P \left(A^T A\right)^{-\frac{1}{2}}\right)$$

and

$$\hat{z}(\lambda) = \left(A^T A + \lambda P\right)^{-1} \left(A^T b - \lambda q\right)$$

The estimate $\hat{p}$ is given by the first 3 elements of $\hat{z}$.

Algorithm 4 Chueng

$$A = \begin{bmatrix} s_1^T & -0.5 \\ \vdots & \\ s_4^T & -0.5 \end{bmatrix}, \quad b = 2\tfrac{1}{2} \begin{bmatrix} \|s_1\|^2 - r_1^2 \\ \vdots \\ \|s_4\|^2 - r_4^2 \end{bmatrix}$$
$$B = \begin{bmatrix} r_1 & & & \\ & \ddots & & \\ & & & r_4 \end{bmatrix}, \quad \Psi = B(B^T I_N)$$
$$P = \begin{bmatrix} 1 & 0 & 0 & 0 \\ 0 & 1 & 0 & 0 \\ 0 & 0 & 1 & 0 \\ 0 & 0 & 0 & 0 \end{bmatrix}, \quad q = \begin{bmatrix} 0 \\ 0 \\ 0 \\ -1 \end{bmatrix}$$

Compute U and Λ from the eigenvalue decomposition

$$\begin{aligned} \left(A^T \Psi^{-1} A\right)^{-1} P &= U \Lambda U^{-1} \\ &= U \begin{bmatrix} \gamma_1 & & & \\ & \gamma_2 & & \\ & & \gamma_3 & \\ & & & 0 \end{bmatrix} U^{-1} \end{aligned}$$

with γ_i the eigenvalues of the matrix $\left(A^T \Psi^{-1} A\right)^{-1} P$, and

$$\begin{aligned} c &= 2U^T q \\ g &= 2U^{-1} \left(A^T \Psi^{-1} A\right)^{-1} q \\ e &= \left(\Psi^{-1} A U\right)^T b \\ f &= U^{-1} \left(A^T \Psi^{-1} A\right)^{-1} A^T \Psi^{-1} b, \end{aligned}$$

Find the absolute of the complex root λ^* closest to zero of the following seven-root equation

$$\begin{aligned} 0 =& c_4 f_4 - \frac{\lambda}{2} c_4 g_4 + \sum_{i=1}^{3} \frac{c_i f_i}{1 + \lambda\gamma_i} - \frac{\lambda}{2} \sum_{i=1}^{3} \frac{c_i g_i}{1 + \lambda\gamma_i} \\ &+ \sum_{i=1}^{3} \frac{e_i f_i \gamma_i}{(1 + \lambda\gamma_i)^2} - \frac{\lambda}{2} \sum_{i=1}^{3} \frac{(e_i g_i + c_i f_i)\gamma_i}{(1 + \lambda\gamma_i)^2} \\ &+ \frac{\lambda^2}{4} \sum_{i=1}^{3} \frac{c_i g_i \gamma_i}{(1 + \lambda\gamma_i)^2}. \end{aligned}$$

and compute the estimate of the constrained weighted least squares

$$\hat{z} = \left(A^T \Psi^{-1} A + \lambda^* P\right)^{-1} \left(A^T \Psi^{-1} b - \frac{\lambda^*}{2} q\right)$$

with the first three elements of $\hat{z}$ as the position estimate $\hat{p}$.

Algorithm 5 Gauss-Newton

1) Calculate an initial guess p_0, a stopping tolerance δ and an iteration upper limit k_{max}. As a starting point, the simple intersection method is chosen. Set $k = 0$.
2) Compute the Jacobian Matrix:

$$J_k(p) = \begin{bmatrix} \frac{s_1 - p}{\|s_1 - p\|}^T \\ \vdots \\ \frac{s_4 - p}{\|s_4 - p\|}^T \end{bmatrix}$$

3) Set $p_{k+1} = p_k + \Delta p_k$, where Δp_k the least square solution is of:

$$\left(\Sigma^{-\frac{1}{2}} \left(h\left(p_k\right) - r\right)\right) \Delta p_k = -\left(\Sigma^{-\frac{1}{2}} J_k\right)$$

4) If stopping condition $\|\Delta p_k\| < \delta$ is not satisfied and $k \leq k_{\max}$, increment k and repeat from Step 2.